High-pressure ferroelastic phase transition in aluminosilicate hollandite

Tiziana Boffa Ballaran,[1,*] Jun Liu,[1] Leonid S. Dubrovinsky,[1] Razvan Caracas,[2] and Wilson Crichton[3]
[1]*Bayerisches Geoinstitut, Universität Bayreuth, D-95440 Bayreuth, Germany*
[2]*Centre National de la Recherche Scientifique, Laboratoire de Sciences de la Terre, UMR 5570, Ecole Normale Supérieure de Lyon, 46 allée d'Italie, 69364 Lyon, France*
[3]*European Synchrotron Radiation Facility, Boîte Postale 220, 38043 Grenoble Cedex 9, France*
(Received 8 October 2009; revised manuscript received 26 October 2009; published 4 December 2009)

We used x-ray synchrotron powder diffraction, Raman spectroscopy, and first-principles calculations to characterize the high-pressure ferroelastic $I4/m$ to $I2/m$ transition of $K_{0.8}Na_{0.2}AlSi_3O_8$ hollandite, a structural prototype of materials used in various applications ranging from immobilization of radioactive wastes to ionic conductors. The transition is second-order in character with an equilibrium transition pressure renormalized by coupling of the soft mode with the spontaneous strain. The variations in the lattice strains and of the frequency of the soft optic mode with pressure have been used to develop a Landau free-energy expansion to describe the elastic constant variations in $K_{0.8}Na_{0.2}AlSi_3O_8$ across the transition.

DOI: 10.1103/PhysRevB.80.214104 PACS number(s): 61.50.Ks, 64.60.Bd, 91.60.Gf

I. INTRODUCTION

Hollandite compounds have been studied extensively by a broad scientific community for several reasons: (i) some hollandite-type oxides are known as one-dimensional (1D) fast conductors for alkali ions;[1,2] (ii) titanates with the hollandite structure exhibit photoelectrochemical properties;[3] (iii) $Ba_x(Al^{3+}Ti^{4+})_8O_{16}$ hollandite is used as a host for the immobilization of radioactive wastes in the mineral assemblage known as SYNROCK (Refs. 4 and 5); and (iv) hollandite-type manganese oxides show ion-sieve properties[6,7] and are possible cathode materials for lithium secondary batteries.[8] The ideal hollandite structure has tetragonal symmetry, $I4/m$, and is composed of edge-sharing octahedra that form double chains parallel to the **c** axis. These octahedral chains, in turn, share corners with neighboring double chains to form a framework structure containing two types of 1D channels that are 1×1 and 2×2 octahedra wide. The 2×2 octahedra wide channels can accommodate large cations with low valences. The general chemical formula of hollandite-type compounds is $A_xB_8O_{16}$ $(x\leq2)$ where A represents ions in the tunnel cavities and B are two- to five-valent cations occupying the octahedral sites. The A-type cations occupying the 2×2 tunnels are ideally located at the intersection of the mirror plane and the fourfold axis (Wyckoff position 2*b*, 0, 0, 1/2). A large variety of chemical species have been reported forming some 30 different end-member compositions[9] with A=Na, Ag, K, Tl, Rb, Cs, Ba, Sr, and Pb; and B=Mg, Cu, Zn, Co, Ni, Al, Ga, Fe, In, Sc, Cr, Si, Ge, Ti, Mn, Sn, and Sb. Many hollandite structures are slightly distorted with a consequent lowering of the symmetry to the monoclinic space group $I2/m$ or even show incommensurate modulations.[10–12] The monoclinic distortion appears to be related to the size of the A cation: if this is too small, the columns of BO_6 octahedra twist to decrease the volume of the tunnels,[13] a case similar to that observed in perovskite structures where the octahedra twist or tilt in order to better accommodate small cations in their A site.

The aluminosilicate hollandite-type structure (with Al and Si occupying the octahedral sites), so far has received relatively little attention, in spite of being a possible host of alkaline elements (such as Na and K) in the Earth's mantle. Silicate hollandite, in fact, is isochemical with alkali feldspars $(Na,K)AlSi_3O_8$ which are among the most abundant minerals in the Earth's crust and whose high-pressure behavior is of great importance for the geophysical and mineral physics communities because feldspar-rich crustal materials may be subducted to a great depth.

Recent *in situ* high-pressure studies of $KAlSi_3O_8$ hollandite[14–17] reported a nonquenchable phase transformation from tetragonal to monoclinic symmetry at about 20 GPa. The high-pressure phase can be indexed with a monoclinic unit-cell (space group $I2/m$) isostructural with $BaMn_8O_{16}$ hollandite. The transition is described by the group subgroup relationship $4/m$ to $2/m$ for which the active representation is Bg of point group $4/m$. Ferroelastic phase transitions of this type are expected to conform to the precepts of Landau theory due to the role of strain in promoting mean-field behavior. However, although Landau theory has been used to describe the behavior of phase transitions occurring in many materials as a function of temperature, very few examples of full determination of Landau potentials can be found for high-pressure transitions.[18,19] This is mainly due to the difficulty in obtaining the whole range of data with the necessary accuracy to determine the coefficients of a full Landau expansion. Here we study the mechanism of the ferroelastic phase transition. We made use of a variety of complementary techniques: high-pressure x-ray diffraction, high-pressure Raman spectroscopy, and first-principles calculations. We derived the Landau free-energy expansion and we studied its variation and the behavior of the elastic constant of $K_{0.8}Na_{0.2}AlSi_3O_8$ across the tetragonal to monoclinic phase transition.

II. EXPERIMENTAL METHODS

The $K_{0.8}Na_{0.2}AlSi_3O_8$ sample was synthesized in a multianvil press at 20 GPa and 1700 °C from a stoichiometric mixture of K_2CO_3, Na_2CO_3, Al_2O_3, and SiO_2 and the composition of the run product was confirmed by microprobe

TABLE I. Unit-cell lattice parameters and standard deviations of tetragonal and monoclinic $K_{0.8}Na_{0.2}AlSi_3O_8$ hollandite at different pressures.

Pressure (GPa)	a (Å)	b (Å)	c (Å)	γ (deg)	V (Å^3)
9.8	9.1640 (6)		2.6987 (2)	90	226.64 (3)
11.1	9.1486 (7)		2.6937 (3)	90	225.45 (3)
12.5	9.1280 (6)		2.6894 (3)	90	224.08 (3)
13.2	9.1147 (8)		2.6898 (4)	90	223.46 (3)
14.6	9.0990 (4)		2.6851 (2)	90	222.31 (2)
16.3	9.0882 (7)		2.6811 (3)	90	221.45 (3)
16.5	9.0769 (7)		2.6815 (3)	90	220.92 (3)
19.3	9.1372 (10)	8.9220 (12)	2.6743 (3)	90.470 (11)	218.01 (4)
18.5[a]	9.1265 (10)	8.9857 (12)	2.6754 (2)	90.528 (14)	219.39 (4)
17.5[a]	9.0988 (11)	9.0259 (12)	2.6787 (3)	90.273 (12)	219.98 (3)
17.0[a]	9.0731 (10)		2.6786 (3)	90	220.51 (4)
21.0	9.1376 (14)	8.8809 (9)	2.6682 (2)	90.795 (11)	216.50 (4)
24.0	9.1505 (8)	8.8089 (9)	2.6613 (1)	91.316 (10)	214.46 (3)
26.6	9.1604 (7)	8.7441 (12)	2.6544 (1)	91.576 (8)	212.54 (3)
26.6	9.1668 (9)	8.7377 (12)	2.6542 (1)	91.477 (12)	212.52 (4)
26.6	9.1622 (90)	8.741 (12)	2.6544 (2)	91.510 (13)	212.51 (4)
29.0	9.1721 (12)	8.6817 (14)	2.6472 (10)	91.553 (14)	210.71 (4)
29.3	9.1778 (13)	8.6585 (10)	2.6451 (8)	91.767 (13)	210.10 (3)
23.2[a]	9.1666 (13)	8.8009 (14)	2.6607 (1)	91.296 (14)	214.59 (4)
13.2[a]	9.1277 (6)		2.6888 (2)	90	224.02 (3)
10.4[a]	9.1581 (4)		2.6966 (2)	90	226.16 (2)
8.2[a]	9.1957 (6)		2.7035 (2)	90	228.61 (3)
5.6[a]	9.2353 (4)		2.7098 (1)	90	231.12 (2)
3.1[a]	9.2768 (5)		2.7168 (1)	90	233.80 (2)
0.7[a]	9.3180 (5)		2.7244 (1)	90	236.54 (2)

[a]Data collected during decompression. Note: uncertainties on pressure are estimated to be on the order of 0.05–0.1 GPa.

analysis. Few grains of hollandite (3–5 μm) were loaded into a 100 μm hole of a steel gasket preindented to a 50 μm thickness and mounted on a membrane digital-to-analog converter (DAC) loaded with He as pressure transmitting medium. A ruby chip was used as internal pressure standard. The $K_{0.8}Na_{0.2}AlSi_3O_8$ hollandite sample was compressed at room temperature up to ~30 GPa and then slowly decompressed to ambient pressure. X-ray powder-diffraction data were collected at room temperature for 300 s at each pressure at the European Synchrotron Radiation Facility (ESRF, Grenoble, France), on beam line ID-27, with a focused monochromatic beam (wavelength=0.264 72 Å, size ~5 $\times$10 μm) and a Mar charge coupled device (CCD) detector. The diffraction images were integrated using the FIT2D software, and lattice parameters were determined by full profile refinements of the diffraction patterns using the GSAS package[20] and the EXPGUI Windows interface.[21] Raman spectra of the same sample were collected at pressures up to 20 GPa at the Bayerisches Geoinstitut, using a Dilor XY system with the 514.5 nm Ar^+ ion laser equipped with a microscope and liquid-nitrogen-cooled CCD detector and a DAC also loaded with He.

III. LATTICE STRAIN

In the x-ray powder-diffraction pattern collected during compression, we observed at ~17–18 GPa peak splitting due to the tetragonal to monoclinic phase transformation. The monoclinic phase was stable up to the maximum pressure reached. In order to keep the group-subgroup relationship between tetragonal and monoclinic phases, we use the monoclinic cell $I2/m$ with c as unique axis, instead of using the preferred setting of b unique reported for several hollandite structures.[5,13] In this way the tunnels are still parallel to the c axis and it is possible to compare directly the unit-cell lattice parameters of the two phases. The unit-cell lattice parameters obtained from the Rietveld refinements of the several diffraction patterns collected at different pressures are listed in Table I for both tetragonal and monoclinic $K_{0.8}Na_{0.2}AlSi_3O_8$ hollandite. The tetragonal to monoclinic phase transformation is characterized by a clear splitting of the a tetragonal axis into the a and b monoclinic axes and by a continuous increase in the angle γ (Fig. 1). No discontinuity appears in the evolution of the c axis and of the unit-cell volume with pressure. An analysis of the "normalized

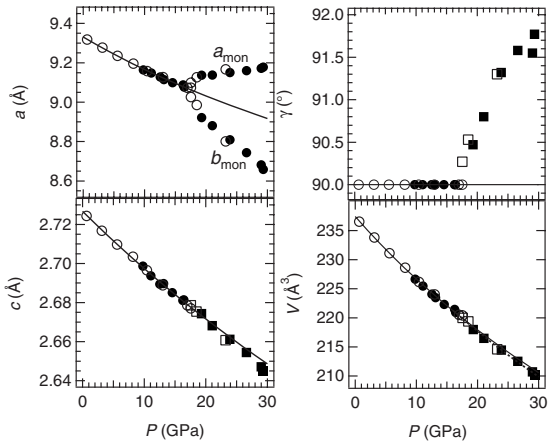

FIG. 1. Unit-cell lattice parameters as a function of pressure of $K_{0.8}Na_{0.2}AlSi_3O_8$ hollandite. Filled and open circles are data of the tetragonal phase in compression and decompression, respectively; solid and open squares are data of the monoclinic phase in compression and in decompression, respectively. Solid curves are BM-II EoS fits of the tetragonal data. Dotted curve is a BM-II EoS fit of the volume of the monoclinic phase.

stress," $F_E = P/3f_E(1+2f_E)^{5/2}$, vs finite strain, $f_E = [(V_0/V)^{2/3}-1]/2$, plot,[22] indicates that the data of both the tetragonal and the monoclinic phase can be fitted with a horizontal line, implying that a second order Birch-Murnaghan (BM-II) equation of state (EoS) is sufficient for fitting the P-V data. The EoS parameters calculated using the software EoSFit52t (Ref. 23) are the following: $V_0=237.3$ (2) Å^3, $K_0=198$ (3) GPa for the tetragonal phase and $V_0=239.4$ (9) Å^3, $K_0=174$ (7) GPa for the monoclinic phase (K' has the implied value of 4). A linearized BM-II EoS has been used to fit the variation in the unit-cell a and c parameters of the tetragonal $K_{0.8}Na_{0.2}AlSi_3O_8$ hollandite. The K_0 values so obtained are then one-third of the inverse of the zero-pressure linear compressibility β_0 of the axes, defined as $\beta_0 = \frac{1}{l_0}(\frac{\delta l}{\delta P})_{P=0}$ in which l_0 is the length of the unit-cell axis at room P. The resulting linearized BM-II EoS parameters obtained are the following: $a_0=9.330$ (3) Å and $K_0=170$ (3) GPa for the a axis, and $c_0=2.7266$ (3) Å and $K_0=290$ (4) GPa for the c axis, indicating an anisotropic linear compressibility with the a axis much more compressible than the c axis. The room pressure bulk modulus of the tetragonal $K_{0.8}Na_{0.2}AlSi_3O_8$ hollandite is very similar to that reported for the tetragonal $KAlSi_3O_8$ hollandite end member,[16] suggesting that the substitution of Na has little effect on the bulk compressibility of hollandite.

The four nonzero lattice strain components associated with the ferroelastic transition are obtained in terms of the unit-cell parameters according to the following expressions:[24,25]

$$e_{1,tot} = \frac{a \sin \gamma}{a_0} - 1; \quad e_{2,tot} = \frac{b}{a_0} - 1;$$

$$e_{3,tot} = \frac{c}{c_0} - 1; \quad \text{and} \quad e_{6,tot} = \frac{a}{a_0}\cos \gamma, \qquad (1)$$

where a, b, c, and γ are the lattice parameters of the monoclinic phase, and a_0 and c_0 are the lattice parameters of the tetragonal phase extrapolated into the stability field of the monoclinic phase using the BM-II EoS linear parameters (Fig. 1). The symmetry-breaking and nonsymmetry-breaking strain components can be separated as: $e_{1,sb} = \frac{e_{1,tot}-e_{2,tot}}{2}$; $e_{1,nsb} = \frac{e_{1,tot}+e_{2,tot}}{2}$; $e_{3,nsb}=e_{3,tot}$; and $e_{6,sb}=e_{6,tot}$. The symmetry-breaking strains transform as R_{active} so that linear coupling with the order parameter Q associated with the phase transformation is expected, whereas the nonsymmetry-breaking strain components should couple with Q^2.[25,26] The nonsymmetry-breaking strains are found to be 1 order of magnitude smaller than the symmetry-breaking strains. The linear variations in the square of the symmetry-breaking strains, $(e_1-e_2)^2$ and e_6^2 with pressure (Fig. 2) is consistent with Q^2 being proportional to P and therefore with a phase-transition second order in character. The linear fits through the data reported in Fig. 2 extrapolated to zero strain give a transition pressure of 17 (1) GPa, i.e., ~2.5 GPa lower than the transition pressure reported for the $KAlSi_3O_8$ hollandite end member.[16]

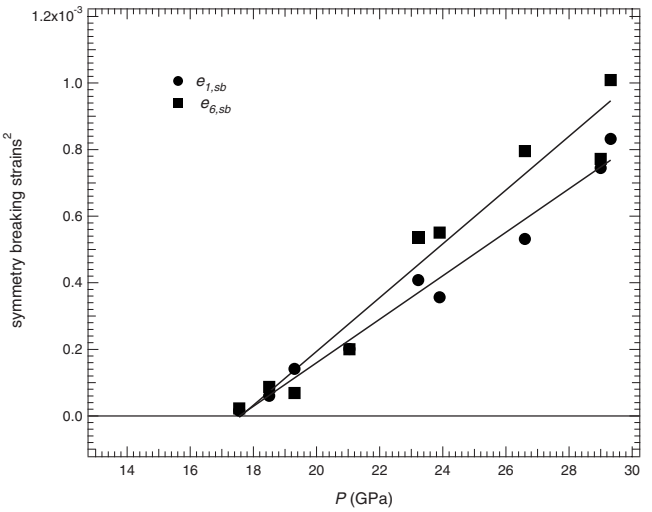

FIG. 2. Variations as a function of pressure of the square of the symmetry-breaking strains (e_1-e_2) and e_6. Solid lines are linear fits through the data given by: $(e_1-e_2)^2=-0.001\ 15(8)+0.000\ 065(4)P$ and $e_6^2=-0.0014(2)+0.000\ 081(7)P$.

IV. B_g RAMAN ACTIVE MODE

Softening of the B_g Raman-active mode at ~219 cm^{-1} due to coupling with the soft acoustic mode driving the transition was observed up to 17 GPa, followed by an increase in wave number up to 20 GPa which is the maximum pressure reached during the experiment. The square of the B_g wave number, ω^2, is expected to vary linearly with the inverse order-parameter susceptibility, $\chi^{-1}=\partial^2 G/\partial Q^2$, e.g., Ref. 27 (Fig. 3). A linear fit through the tetragonal data extrapolated to zero gives a P_c (i.e., the critical pressure at which ω^2 becomes zero) of 312 GPa. The trends of the ω^2 of the high-symmetry and low-symmetry data meet at a renormalized transition pressure $P_c^*=17$ GPa which is in excellent agreement with that obtained from the x-ray diffraction data.

V. BARE ELASTIC CONSTANTS

The elastic constants have been calculated from first principles for the $K_{0.8}Na_{0.2}AlSi_3O_8$ tetragonal hollandite at pres-

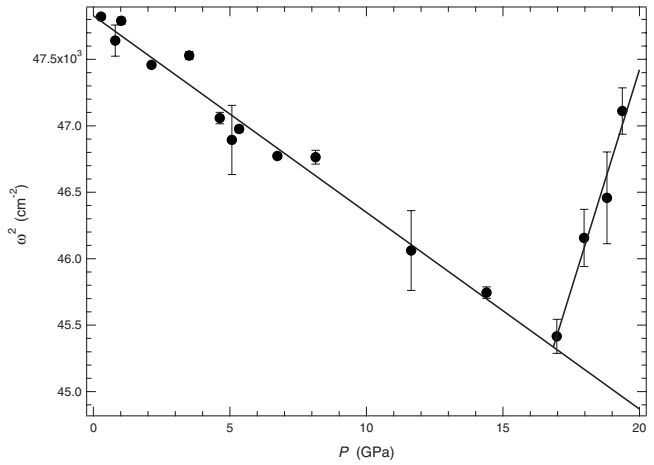

FIG. 3. Variation in the wave number squared for the B_g Raman-active mode through the tetragonal to monoclinic phase transition. The straight lines through the tetragonal and monoclinic data intersect at $P_c^*=17$ GPa.

sures of 0, 5, 10, and 20 GPa.[34] The pressure dependence of C_{33}^0, C_{13}^0, C_{44}^0, C_{66}^0, and C_{16}^0 has been determined using a linear fit through the calculated data and is reported in Table II. The combination of the elastic constants $(C_{11}-C_{12})$ has the symmetry properties of the active representation for the phase transition, hence, the values of C_{11} and C_{12} calculated for tetragonal hollandite include the influence of the $I4/m$ to $I2/m$ transition and cannot be used directly as bare elastic constants. We determined the values of C_{11}^0 and C_{12}^0 according to the expression[28–30]

$$(C_{11}-C_{12})=(C_{11}^0-C_{12}^0)\left(\frac{P-P_c^*}{P-P_c}\right) \tag{2}$$

setting $(C_{11}-C_{12})=116$ at room pressure as obtained from the calculated elastic constants. Moreover we assumed that C_{11}^0 and C_{12}^0 have the same positive slope with pressure and therefore $(C_{11}^0-C_{12}^0)$ is independent of pressure. $(C_{11}+C_{12})$ has the symmetry properties of the identity representation and therefore is not expected to deviate from $(C_{11}^0+C_{12}^0)$ in the high-symmetry phase. The calculated values of C_{11} and C_{12} have therefore been summed to give the evolution of $(C_{11}^0+C_{12}^0)=482+7.33P$ and combined with the value of $(C_{11}^0-C_{12}^0)$ to obtain the values of C_{11}^0 and C_{12}^0 reported in Table II.

TABLE II. Values of bare elastic constants calculated for $K_{0.8}Na_{0.2}AlSi_3O_8$ hollandite, transition pressure, coupling coefficients, and Landau coefficients. All values are in GPa units except for a which is dimensionless.

Bare elastic constants	Landau coefficients
$C_{11}^0=1305+3.66P$	$P_c^*=17$
$C_{33}^0=556+4.55P$	$P_c=312$
$C_{12}^0=-824+3.66P$	$\lambda_1=8.52$
$C_{13}^0=112+1.7P$	$\lambda_2=-85.97$
$C_{44}^0=168+1.05P$	$\lambda_3=21.4$
$C_{66}^0=111+0.5P$	$\lambda_6=3.75$
$C_{16}^0=48+1.28P$	$a=-0.02354$
$C_{26}^0=-48-1.28P$	$b=4.3285$

VI. LANDAU FREE-ENERGY POTENTIAL

The Landau free-energy expansion difference between the paraelastic (i.e., tetragonal) and the ferroelastic (i.e., monoclinic) phases of the $K_{0.8}Na_{0.2}AlSi_3O_8$ hollandite for a second-order transition can be written[31] as

$$\begin{aligned}\Delta G=&\frac{1}{2}a(P-P_c)Q^2+\frac{1}{4}bQ^4+\lambda_1(e_1+e_2)Q^2+\lambda_2(e_1-e_2)Q\\&+\lambda_3e_3Q^2+\lambda_4(e_4^2-e_5^2)Q^2+\lambda_5e_4e_5Q+\lambda_6e_6Q\\&+\frac{1}{4}(C_{11}^0-C_{12}^0)(e_1-e_2)^2+\frac{1}{4}(C_{11}^0+C_{12}^0)(e_1+e_2)^2\\&+C_{13}^0(e_1+e_2)e_3+\frac{1}{2}C_{33}^0e_3^2+\frac{1}{2}C_{44}^0(e_4^2+e_5^4)+\frac{1}{2}C_{66}^0e_6^2\\&+C_{16}^0(e_1-e_2)e_6,\end{aligned} \tag{3}$$

where Q is the driving order parameter associated with the phase transition, a and b are Landau coefficient, P_c is the critical pressure, e_1-e_6 are spontaneous strains, $\lambda_1-\lambda_6$ are strain/order-parameter coupling coefficients, and C_{ik} are the bare elastic constants of the tetragonal phase. The strain components e_4 and e_5 are strictly zero in the monoclinic phase. The equilibrium variations in the symmetry-breaking strains (e_1-e_2) and e_6 and of the nonsymmetry-breaking strains e_1+e_2 and e_3, and hence, their variation with Q can be obtained deriving the Landau potential [Eq. (3)] with respect to the strain components (see for review, Ref. 30). The following expressions are thus obtained:

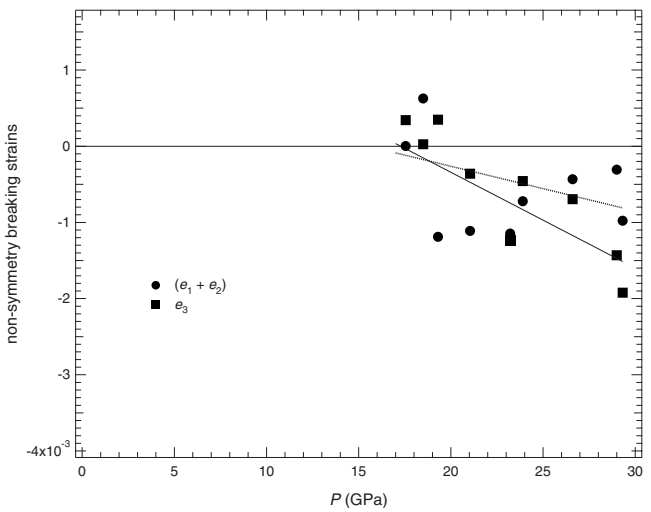

FIG. 4. Variations as a function of pressure of the nonsymmetry-breaking strains (e_1+e_2) and e_3. Solid lines are linear fits through the data constrained to give a critical pressure of about 17 GPa. The fits are given by: $(e_1+e_2)=0.0009(5)-0.000\,06(2)P$ (dotted line) and $e_3=0.000\,22(6)-0.000\,13(2)P$ (solid line).

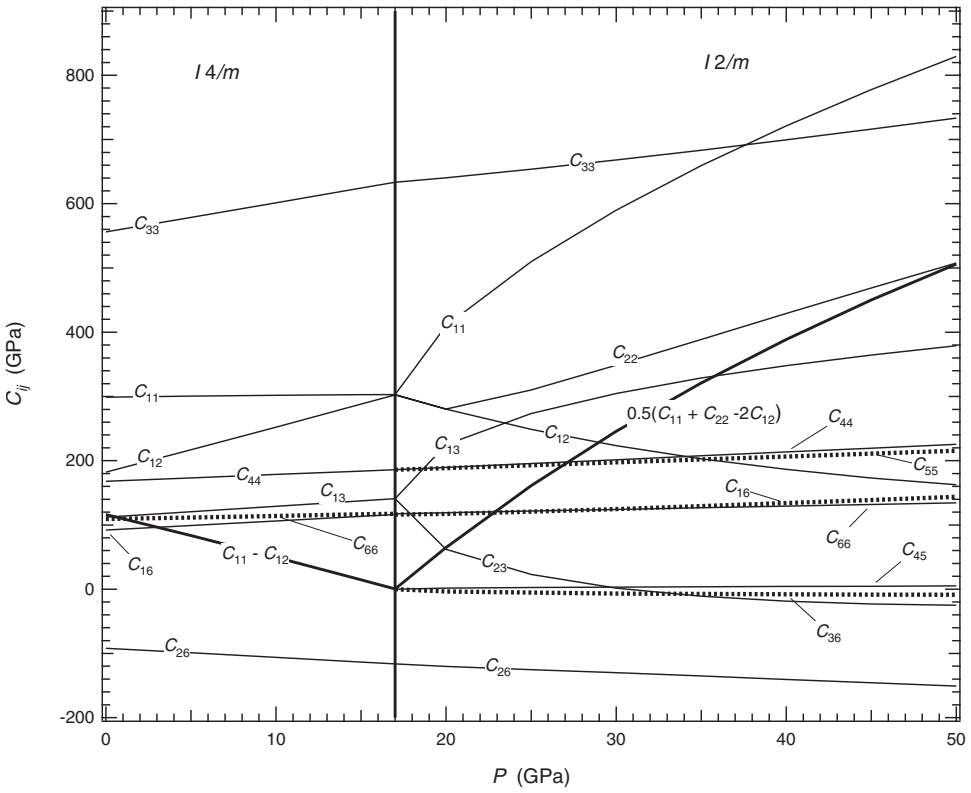

FIG. 5. Variations with pressure of the individual elastic constants given by the expressions in Table III and values of the coefficients and bare elastic constants in Table II.

$$(e_1 - e_2) = \frac{2C_{16}^0\lambda_6 - 2C_{66}^0\lambda_2}{C_{66}^0(C_{11}^0 - C_{12}^0) - 2C_{16}^{02}}Q, \tag{4}$$

$$e_6 = \frac{2C_{16}^0\lambda_2 - (C_{11}^0 - C_{12}^0)\lambda_6}{C_{66}^0(C_{11}^0 - C_{12}^0) - 2C_{16}^{02}}Q, \tag{5}$$

$$(e_1 + e_2) = \frac{2C_{13}^0\lambda_3 - 2C_{33}^0\lambda_1}{C_{33}^0(C_{11}^0 + C_{12}^0) - 2C_{13}^{02}}Q^2, \tag{6}$$

$$e_3 = \frac{2C_{13}^0\lambda_1 - (C_{11}^0 + C_{12}^0)\lambda_3}{C_{33}^0(C_{11}^0 + C_{12}^0) - 2C_{13}^{02}}Q^2. \tag{7}$$

Substituting these values into free-energy Landau expansion (3) we obtain a renormalized fourth-order coefficient b^* given by

$$b^* = b + 2\frac{2C_{33}^0\lambda_1^2 - 4C_{13}^0\lambda_1\lambda_3 + \lambda_3^2(C_{11}^0 + C_{12}^0)}{2C_{13}^{02} - C_{33}^0(C_{11}^0 + C_{12}^0)} \tag{8}$$

and a pressure dependence of the order parameter given by

$$Q^2 = \frac{a}{b^*}(P_c^* - P), \tag{9}$$

where P_c^* is the renormalized transition pressure observed in the x-ray and Raman experiments.

In contrast with phase transitions occurring as a function of temperature for which the order parameter is usually defined as having the value of 1 at 0 K, phase transitions occurring as a function of pressure require an arbitrary choice of the absolute value of the order parameter. In the case of hollandite we have chosen $Q=0.5$ at $P=50$ GPa, whereas $Q=0$ for the high-symmetry phase as in the normal manner. From the linear fits reported in Fig. 2, $(e_1-e_2)=0.0458$ and $e_6=-0.0515$ [note that from Eq. (1) e_6 is negative] at $P=50$ GPa. The nonsymmetry-breaking strains show a larger scatter due to their values being on the order of the uncertainties of the measurements, however they can still be linearly extrapolated to 50 GPa giving $(e_1+e_2)=-0.0021$ and $e_3=-0.0063$ (Fig. 4).

The Landau coefficients reported in Table II can then be obtained by analytically solving Eqs. (4)–(9) substituting the strain values and the bare elastic constant values at 50 GPa and the values P_c^*. The overall elastic behavior of $K_{0.8}Na_{0.2}AlSi_3O_8$ hollandite through the tetragonal to monoclinic phase transition (Fig. 5) can then be described following the individual elastic constant variations with pressure (Table III) according to:[26,32]

$$C_{ik} = C_{ik}^0 - \sum \frac{\partial^2 G}{\partial e_i\,\partial Q}\left(\frac{\partial^2 G}{\partial Q^2}\right)^{-1}\frac{\partial^2 G}{\partial e_k\,\partial Q}. \tag{10}$$

Softening of the tetragonal $(C_{11}-C_{12})$ is clearly observed and its value goes to zero at the transition pressure of 17 GPa. The value of $0.5(C_{11}+C_{22}-2C_{12})$ also tends to zero as the transition pressure is approached from the high-pressure site. We can expect, therefore, that the variation with pressure of the shear modulus, as well as of the P and S waves for aluminosilicate hollandite will show a marked softening as the transition point is approached from both the low- and high-pressure sides.

Since we have allowed the bare elastic constants to be pressure dependent, the evolution of the order parameter through a pressure-driven phase transition differs from that

TABLE III. Expressions for the elastic constant of $K_{0.8}Na_{0.2}AlSi_3O_8$ hollandite. Note: the order-parameter susceptibility is given by: $\chi=1/[a(P-P_c)]$ for $P<P_c^*$ and $\chi=1/[2a\frac{b}{b^*}(P_c^*-P)+a(P_c^*-P_c)]$ for $P>P_c^*$.

Tetragonal structure ($I4/m$)	Monoclinic structure ($I2/m$)
$C_{11}=C_{22}=C_{11}^0-\lambda_2^2\chi$	$C_{11}=C_{11}^0-(\lambda_2^2+4\lambda_1^2Q^2+4\lambda_1\lambda_2Q)\chi$
	$C_{22}=C_{11}^0-(\lambda_2^2+4\lambda_1^2Q^2-4\lambda_1\lambda_2Q)\chi$
$C_{33}=C_{33}^0$	$C_{33}=C_{33}^0-4\lambda_3^2Q^2\chi$
$C_{12}=C_{12}^0+\lambda_2^2\chi$	$C_{12}=C_{12}^0-(4\lambda_1^2Q^2-\lambda_2^2)\chi$
$C_{13}=C_{23}=C_{13}^0$	$C_{13}=C_{13}^0-(2\lambda_2\lambda_3Q+4\lambda_1\lambda_3Q^2)\chi$
	$C_{23}=C_{13}^0-(-2\lambda_2\lambda_3Q+4\lambda_1\lambda_3Q^2)\chi$
$C_{16}=-C_{26}=C_{16}^0-\lambda_2\lambda_6\chi$	$C_{16}=C_{16}^0-(2\lambda_1\lambda_6Q+\lambda_2\lambda_6)\chi$
	$C_{26}=-C_{16}^0-(2\lambda_1\lambda_6Q-\lambda_2\lambda_6)\chi$
	$C_{36}=-2\lambda_3\lambda_6Q\chi$
$C_{11}-C_{12}=(C_{11}^0-C_{12}^0)-2\lambda_2^2\chi$	$C_{11}-C_{12}=(C_{11}^0-C_{12}^0)-(2\lambda_2^2+4\lambda_1\lambda_2Q)\chi$
$C_{11}+C_{12}=(C_{11}^0+C_{12}^0)$	$C_{11}+C_{12}=(C_{11}^0+C_{12}^0)-(8\lambda_1^2Q^2+4\lambda_1\lambda_2Q)\chi$
	$\bar{C}_{11}-\bar{C}_{12}=\frac{1}{2}(C_{11}+C_{22}-2C_{12})=(C_{11}^0-C_{12}^0)-2\lambda_2^2\chi$
	$\bar{C}_{11}+\bar{C}_{12}=\frac{1}{2}(C_{11}+C_{22}+2C_{12})=(C_{11}^0+C_{12}^0)-8\lambda_1^2Q^2\chi$
	$\bar{C}_{16}=\frac{1}{2}(C_{16}-C_{26})=C_{16}^0-\lambda_2\lambda_6\chi$
	$(C_{16}+C_{26})=-4\lambda_1\lambda_6Q\chi$
$C_{44}=C_{55}=C_{44}^0$	$C_{44}=C_{44}^0+2\lambda_4Q^2$
	$C_{55}=C_{44}^0-2\lambda_4Q^2$
	$C_{45}=\lambda_5Q$
$C_{66}=C_{66}^0-\lambda_6^2\chi$	$C_{66}=C_{66}^0-\lambda_6^2\chi$

through a temperature-driven phase transition. The fourth-order Landau coefficient b^* becomes pressure dependent due to the pressure dependence of the bare elastic constant [Eq. (8)], as a consequence the pressure dependence of Q^2 of a second-order transition and hence those of $(e_1-e_2)^2$ and e_6^2 are not expected to be exactly linear, although the scatter of the data are such that such behavior cannot be clearly detected in the experimental data. The order-parameter susceptibility in the monoclinic phase also will have some nonlinearity due to the pressure dependence of b^* and as a consequence ω^2 of the soft mode should recover nonlinearly after the transition, although the pressure range investigated here (Fig. 3) is too limited to really detect such nonlinearity. Finally, substitution of Na into the $KAlSi_3O_8$ hollandite structure decreases the transition pressure with respect to that observed for the end member [20 GPa (Ref. 16)]. Ignoring higher-order coupling terms between composition and order parameter, we can consider the effect of composition on the Landau free-energy expansion according to

$$\Delta G = \frac{1}{2}a(P - P_c^{*\prime})Q^2 + \frac{1}{4}b^*Q^4, \tag{11}$$

where $P_c^{*\prime}=17=20+\lambda_7 X_{Na}$ with $\lambda_7=-15$ GPa being the coupling coefficient between order parameter and the molar content of Na, X_{Na}, in $KAlSi_3O_8$ hollandite.

The Landau free-energy expansion gives the free energy of the hollandite monoclinic phase relative to the free energy of the tetragonal phase as a function of pressure once all the coefficients have been determined. Using the values reported in Table II we obtain the excess energy ΔG in J/m^3 that we converted in J/mol using the molar volume of monoclinic hollandite calculated at the different pressures using the BM2-EoS. Assuming similar entropy contributions of the tetragonal and monoclinic phases due to the close similarity of their structure, the total excess free energy calculated in this study (Fig. 6) is in good agreement with the values of excess enthalpy calculated for the tetragonal to monoclinic transition of the end-member $KAlSi_3O_8$ hollandite (Fig. 2 in Ref.

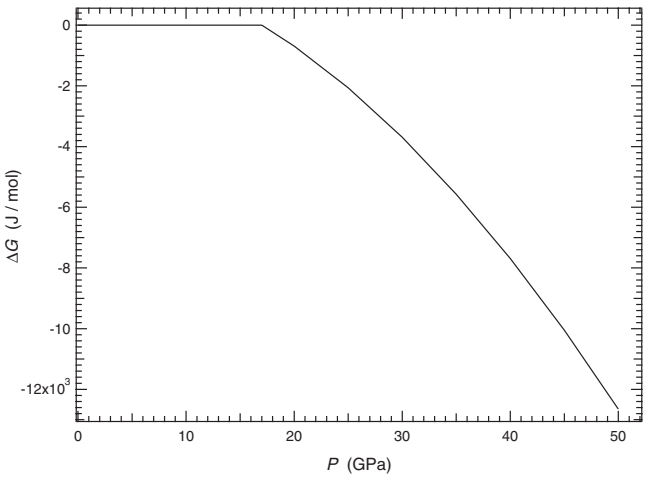

FIG. 6. Excess free energy ΔG as for the tetragonal to monoclinic transition of $K_{0.8}Na_{0.2}AlSi_3O_8$ hollandite as calculated from Eq. (3).

33). We successfully combined accurate experimental data and computational results into a comprehensive Landau expansion to show that the ferroelastic phase transition in hollandite is due to the coupling of the soft acoustic mode with the optic B_g mode and with the (e_1-e_2) and e_6 symmetry-breaking strain components.

ACKNOWLEDGMENTS

Financial support was provided by the DFG, Grant No. BO 2550/1-1. R.C. acknowledges support from the Visitors Program of the Bayerisches Geoinsitut. Thanks are due to M. A. Carpenter for his helpful discussion.

*Corresponding author. tiziana.boffa-ballaran@uni-bayreuth.de

[1] T. Takahashi and K. Kuwabara, Electrochim. Acta **23**, 375 (1978).
[2] Shinzo Yoshikado, Yuichi Michiue, Yoshito Onoda, and Mamoru Watanabe, Solid State Ionics **136-137**, 371 (2000).
[3] L. G. J. De Haart, A. J. Vries, and G. Blasse, J. Solid State Chem. **59**, 291 (1985).
[4] A. E. Ringwood, S. E. Kesson, N. G. Ware, W. O. Hibberson, and A. Major, Geochem. J. **13**, 141 (1979).
[5] R. W. Cheary, Acta Crystallogr., Sect. B: Struct. Sci. **42**, 229 (1986).
[6] Roberto N. DeGuzman, Yan-Fei Shen, Edward J. Neth, Steven L. Suib, Chi-Lin O'Young, Steven Levine, and John M. Newsam, Chem. Mater. **6**, 815 (1994).
[7] Qi Feng, Hirofumi Kanoh, Yoshitaka Miyai, and Kenta Ooi, Chem. Mater. **7**, 148 (1995).
[8] S. Bach, J. P. Pereire-Ramos, and N. Baffier, Solid State Ionics **80**, 151 (1995).
[9] H. Pentinghaus, Phys. Chem. Miner. **3**, 85 (1978).
[10] F. C. Mijlhoff, D. J. W. Ijdo, and H. W. Zandbergen, Acta Crystallogr., Sect. B: Struct. Sci. **41**, 98 (1985).
[11] R. Caracas, J. Appl. Crystallogr. **35**, 120 (2002).
[12] M. L. Carter and R. L. Withers, J. Solid State Chem. **178**, 1903 (2005).
[13] J. E. Post, R. B. Von Dreele, and P. R. Buseck, Acta Crystallogr., Sect. B: Struct. Crystallogr. Cryst. Chem. **38**, 1056 (1982).
[14] Y. Sueda *et al.*, Geophys. Res. Lett. **31**, L23612 (2004).
[15] Norimasa Nishiyama, Robert Paul Rapp, Tetsuo Irifune, Takeshi Sanehira, Daisuke Yamazaki, and Ken-ichi Funakoshi, Phys. Chem. Miner. **32**, 627 (2005).
[16] Tristan Ferroir, Tsuyoshi Onozawa, Takehiko Yagi, Sebastien Merkel, Nobuyoshi Miyajima, Norimasa Nishiyama, Tetsuo Irifune, and Takumi Kikegawa, Am. Mineral. **91**, 327 (2006).
[17] N. Hirao, E. Ohtani, T. Kondo, T. Sakai, and T. Kikegawa, Phys. Earth Planet. Inter. **166**, 97 (2008).
[18] W. Schranz, A. Tröster, J. Koppensteiner, and R. Miletich, J. Phys.: Condens. Matter **19**, 275202 (2007).
[19] M. A. Carpenter, R. J. Hemley, and H.-K. Mao, J. Geophys. Res. **105**, 10807 (2000).
[20] A. Larson and R. B. Van Dreele (Los Alamos National Laboratory, NM, 1994).
[21] B. H. Toby, J. Appl. Crystallogr. **34**, 210 (2001).
[22] R. J. Angel, in *High-Temperature and High-Pressure Crystal Chemistry*, edited by R. M. Hazen and R. T. Downs (Mineralogical Society of America, Chantilly, VA, 2000), Vol. 41, p. 35.
[23] R. J. Angel (Virginia Tech, VA, 2002).
[24] W. I. F. David and I. G. Wood, J. Phys. C **16**, 5127 (1983).
[25] M. A. Carpenter, E. K. H. Salje, and A. Graeme-Barber, Eur. J. Mineral. **10**, 621 (1998).
[26] W. I. F. David, J. Phys. C **16**, 5093 (1983).
[27] A. D. Bruce and R. A. Cowley, *Structural Phase Transition* (Taylor and Francis, Philadelphia, PA, 1981).
[28] R. Feile, A. Loidl, and K. Knorr, Phys. Rev. B **26**, 6875 (1982).
[29] K. Knorr, A. Loidl, and J. K. Kjems, Physica B **136**, 311 (1986).
[30] M. A. Carpenter and E. K. H. Salje, Eur. J. Mineral. **10**, 693 (1998).
[31] H. T. Stokes and D. M. Hatch, *Isotropy Subgroups of the 230 Crystallographic Space Groups* (World Scientific Publishing Co. Ptc. Ltd., River Edge, NJ, 1988).
[32] J. C. Slonczewski and H. Thomas, Phys. Rev. B **1**, 3599 (1970).
[33] M. Mookherjee and G. Steinle-Neumann, Earth Planet. Sci. Lett. **288**, 349 (2009).
[34] R. Caracas and Boffa Ballaran (unpublished).